Erythropoietin supplementation ameliorates the immunological and hematological deficiencies of lysinuric protein intolerance in mice

Judith Giroud-Gerbetant[1,2*], Fernando Sotillo[1*], Jorge Couso[3], Antonio Zorzano[1,4,5], Mayka Sanchez[6], Günter Weiss[7], Manuel Palacín[1,2,4#] and Susanna Bodoy[1,2,8#]

[1]Institute for Research in Biomedicine (IRB) Barcelona, The Barcelona Institute of Science and Technology (BIST), Barcelona, Spain; [2]Centro de Investigación Biomédica en Red Enfermedades Raras (CIBERER), Barcelona, Spain; [3]Institute of Predictive and Personalized Medicine of Cancer, Badalona, Spain; [4]Department of Biochemistry and Molecular Biomedicine, University of Barcelona, Barcelona, Spain; [5]Centro de Investigación Biomédica en Red Diabetes y Enfermedades Metabólicas (CIBERDEM), Spain; [6]Faculty of Medicine and Health Sciences. Universitat Internacional de Catalunya (UIC), Sant Cugat, Spain; [7]Department of Internal Medicine II (Infectious Diseases, Immunology, Rheumatology and Pneumology), Medical University of Innsbruck, Innsbruck, Austria; [8]Department of Biosciences, University of Vic - Central University of Catalonia, Vic, Spain.

[*]These authors contributed equally

Key words: y^+LAT1, arginine, iron metabolism, macrophage, red blood cells

Correspondence: mpalacin@irbbarcelona.org (M.P.), susanna.bodoy@irbbarcelona.org (S.B.)

Abstract

SLC7A7 encodes for y^+LAT1, a cationic amino acid transporter expressed on the basolateral membrane of epithelial cells and macrophages. Mutations in human *SLC7A7* cause lysinuric protein intolerance (LPI), a rare autosomal disorder with a variety of clinical symptoms. Citrulline and a low protein diet are widely used to treat the main symptoms of LPI; however, the hematological and immunological abnormalities in LPI remain poorly understood and difficult to manage by established treatments. Here, we show that erythropoietin levels are significantly diminished in mice lacking *Slc7a7*, which reduces the number of erythroblast precursors, resulting in mature red blood cells with a smaller mean corpuscular volume. *Ex vivo* analysis demonstrated that erythrocytes from *Slc7a7*-deficient mice were phagocytosed more by bone marrow-derived macrophages. Gene expression analysis of sorted red pulp macrophages (RPMs) from *Slc7a7*-deficient mice indicated that this cell population had higher erythrophagocytic activity, but preserved heme catabolic activity. The increase in erythrophagocytosis resulted in iron accumulation in macrophages and tissues, and ultimately led to RPM apoptosis. Surprisingly, ablation of *Slc7a7* in myeloid cells failed to trigger tissue iron accumulation or changes in the RPM population, indicating that the expression of this gene in macrophages is not key for the development of iron accumulation in tissue. Finally, restoration of serum erythropoietin levels in *Slc7a7*-deficient mice re-established normal erythropoiesis and erythrophagocytosis and prevented the accumulation of iron in tissues. Thus, erythropoietin has a fundamental role in the immune-hematological alterations of LPI in mice, revealing a new crucial role for this hormone in this disease.

Introduction

Lysinuric protein intolerance (LPI, MIM 222700) is a rare autosomal recessive disease caused by mutations in *SLC7A7* (solute carrier family 7), which encodes for y^+LAT1 (Palacín et al. 2001; Torrents et al. 1999), a light subunit of the heterodimeric amino acid transporter family (Fotiadis, Kanai, and Palacín 2013) that mediates the exchange of the cationic amino acids (CAAs) arginine, ornithine or lysine with neutral amino acids plus sodium across the basolateral membrane of epithelial cells (Palacín et al. 2005). Mutations in *SLC7A7* result in the defective transport of CAAs, resulting in reduced levels in plasma and elevated levels in urine (Palacín, Borsani, and Sebastio 2001). LPI causes a variety of symptoms, of which the more recurrent are vomiting, failure to thrive, and hepatosplenomegaly (enlargement of both the liver and spleen); the most severe symptoms include lung complications, hematological and immunological abnormalities and kidney failure (Ogier de Baulny, Schiff, and Dionisi-Vici 2012). Standard of care treatment for patients with LPI is a low protein-based diet supplemented with oral citrulline (Simell 2001), which is converted to arginine in renal epithelial cells, thereby correcting defects in the urea cycle and hyperammonemia (Dhanakoti et al. 1990). Of note, y^+LAT1 also mediates arginine transport in non-polarized cells including human monocyte-derived macrophages (Rotoli et al. 2020) and alveolar macrophages (Rotoli et al. 2018).

Macrophages are considered to be key for the immune and hematological abnormalities of LPI. For instance, erythroblastophagocytosis (the process of erythroblast phagocytosis) has been reported in some patients with LPI (Dionisi-Vici et al. 1998; Parenti et al. 1995). Hematological complications can also include microcytic and/or hypochronic anemia, hemophagocytic lymphohistiocytosis and loss of megakaryocyte populations (Duval et al. 1999; Korman et al. 2002; Noguchi and Takahashi 2019). However, the most life-threatening complications (pulmonary alveolar proteinosis and end-stage kidney failure) are highly heterogeneous among patients (Ogier de Baulny et al. 2012).

Erythropoiesis, the process of red blood cell (RBC) generation, occurs in the bone marrow (BM), where CD169^{+} macrophages and cytokines orchestrate erythrocyte differentiation and maturation (Chow et al. 2013). RBC maturation is a coordinated process involving specific components such as hemoglobin, ferritin, iron, and erythropoietin (Epo). During RBC recycling, red pulp macrophages (RPMs) and Kupffer cells (resident liver macrophages) phagocytose senescent RBCs, triggering hemoglobin breakdown and, ultimately, iron recycling and release (Klei et al. 2017). In this regard, patients with LPI who develop hemophagocytic lymphohistiocytosis present hyperferritinemia (Ogier de Baulny et al. 2012).

Erythropoietin is a glycoprotein that is synthesized mainly in the kidney (Broxmeyer 2013). Binding of erythropoietin to its receptor stimulates a downstream signaling cascade, including transcription factors such as GATA1 and TAL1 that promotes cell survival, proliferation and differentiation, specifically at the burst-forming unit-erythroid and colony-forming unit-erythroid stages of BM erythropoiesis. Erythropoietin can also trigger erythropoiesis in the spleen under erythropoietic stress (Paulson et al. 2020). Erythropoietin synthesis is regulated principally *via* feedback mechanisms involving oxygen, and systemic hypoxia ensures proper oxygen distribution by enhancing RBC generation. Accordingly, defects in erythropoietin production caused by genetic alterations or secondary to disease, for example, chronic kidney disease, result in impaired RBC production and anemia.

We sought to uncover the mechanisms responsible for the immune and hematological complications in LPI by investigating whether genetic deficiency of *Slc7a7* in mice (a model of human LPI) impacts erythropoiesis and/or iron homeostasis. Through this analysis, we found that shortage of erythropoietin in *Slc7a7* deficient mice causes hyperefficient erythropoiesis and reduced RBC size, which leads to increased erythrophagocytosis and iron redistribution.

Results

Deficiency of *Slc7a7* reduces erythrocyte size and drives tissue iron redistribution

Hypochromic and microcytic anemia has been reported in patients with LPI (Ogier de Baulny et al. 2012), but the mechanism(s) by which this develops remain elusive. Evidence that CAA transport might be necessary for RBC homeostasis comes from a study in mice showing that a germ-line mutation in mCAT-1, a CAA transporter, results in severe anemia (Perkins et al. 1997).

To investigate the hematological abnormalities of LPI, we used an inducible mouse *Slc7a7*-knockout model (Bodoy et al. 2019), where Cre recombinase is expressed ubiquitously after tamoxifen administration. As expected, the kidney expression of y^+LAT1 was substantially lower in *Slc7a7*-deficent mice than in control mice (*Slc7a7*$^{+/+}$), which was accompanied by a loss of arginine in plasma and elevated levels in urine (data not shown) (Bodoy et al. 2019). Also, relative spleen weight was significantly lower in *Slc7a7*-deficent mice than in control littermates, whereas no changes were observed for the relative weight of the gastrocnemius, kidney and liver (Supplementary Figure 1A-D). We next performed blood analysis to question whether *Slc7a7* deletion triggers microcytic anemia. Mean corpuscular volume (MCV) and mean corpuscular hemoglobin were significantly lower in *Slc7a7*-deficient mice than in controls, but no differences were evident in hemoglobin concentration, RBC count or hematocrit (Table 1). Microcytic anemia is typically associated with iron deficiency (Zhu et al. 2008); however, some hematological disorders such as hemolytic anemia and hemochromatosis are linked to iron overload (Camaschella et al. 2000; Priwitzerova et al. 2005). Because iron overload and hyperferritinemia have been reported in some patients with LPI (Ceruti et al. 2007; Ogier de Baulny et al. 2012), we evaluated the presence of iron in tissues to directly assess whether *Slc7a7*-deficient mice develop iron redistribution. Results showed that iron levels in spleen, BM, liver and kidney sections were significantly higher in *Slc7a7*-knockout mice than in control mice (Figure 1A and Supplementary Figure 1E). These findings were further confirmed by the measurement of total iron content in spleen and liver, which was significantly higher in *Slc7a7*-deficient mice (Supplementary Figure 1F-G). We then

studied the factors influencing tissue iron redistribution, finding evident hyperferritinemia in *Slc7a7*-knockout mice (Figure 1B). Because hyperferritinemia is often associated with inflammation (Kawasumi et al. 2014; Rosário et al. 2013) we also evaluated the plasma levels of interleukin (IL)-6, a marker of systemic inflammation. Unexpectedly, control and *Slc7a7*-deficient mice showed similar levels of IL-6 (Figure 1C). Moreover, microarray analysis of sorted RPMs revealed a downregulation of inflammatory-related pathways in *Slc7a7*-deficient mice as compared with control mice (Table 2), excluding systemic inflammation as a plausible cause of the hyperferritinemia (Theurl et al. 2016).

As *Slc7a7* is expressed in macrophages, we hypothesized that iron accumulation might be directly linked to these cells. Histological analysis of spleen sections revealed the accumulation of iron in macrophages from *Slc7a7*-deficient mice but not from control mice (Figure 1D). Overall, the data indicate that *Slc7a7*-deficient mice have a reduced RBC size and that loss of *Slc7a7* drives iron redistribution, as reflected by iron overload in tissues.

Slc7a7-deficient mice have a reduced red pulp macrophage population with evident apoptosis

Because RPMs are responsible for iron recycling and homeostasis (Klei et al. 2017), we next analyzed this cell population in mice. By flow cytometry, we found that the number of monocytes (F4/80^{lo}CD11b^{hi}) RPMs (F4/80^{hi}CD11b^{lo}) in the spleen was significantly lower in *Slc7a7*-deficient mice than in control mice (Figure 2A and Supplementary Figure 2A), and this was consistent with lower F4/80 positive staining in spleen sections from *Slc7a7*-deficient animals (Figure 2B) and a significant and considerable decrease in the number of peripheral blood monocytes (Figure 2C). We then evaluated whether the substantial loss of the RPM population was associated with an increase in apoptosis. We found higher levels of the expression of annexin V in RPMs from *Slc7a7*-deficient mice (Figure 2D and Supplementary Figure 2B).

To further define the mechanisms underlying iron overload and RPM apoptosis, we compared the transcriptome profiles of sorted RPMs from *Slc7a7*-deficient mice and control mice. Analysis revealed the differential expression of key RPM-associated genes (Haldar et

al. 2014; Kohyama et al. 2009) in *Slc7a7*-deficient RPMs (Figure 2E), further pointing to impaired RPM activity. RPMs are highly specialized erythrophagocytic cells with several genes proposed as master regulators of their function and iron homeostasis (Kohyama et al. 2009). Gene expression analysis revealed that levels of both *CD163* and *SpiC* were significantly higher in *Slc7a7*-deficient RPMs than in control RPMs (Figure 2F). *CD163* is a hemoglobin-haptoglobin scavenger receptor and *Spic* is the master regulator of RPM differentiation. Increased hemoglobin intake has been reported to stimulate heme oxygenase (*Hmox1)* gene expression (Olonisakin et al. 2021); however, no changes were observed in *Hmox1* expression in sorted RPMs from the two groups of mice, and the expression of other RPM-associated genes (*Treml4*, *Vcam1* and *Slc40a1*) was also comparable (Figure 2F). The overall gene expression profile of *Slc7a7*-deficient RPMs pattern suggested that erythrophagocytosis was elevated in *Slc7a7*-deficient mice in the absence of *Hmox1* upregulation. FPN1 is the only known iron exporter in macrophages (Drakesmith, Nemeth, and Ganz 2015) and its expression can be regulated at the transcriptional and translational levels. Microarray and gene expression analysis revealed that FPN1 (*Slc40a1*) gene levels were unchanged in *Slc7a7*-deficient RPMs (Figure 2E and 2F); however, western blotting analysis of whole spleen extracts revealed significantly lower levels of FPN1 protein in *Slc7a7*-deficient mice (Figure 2G). Contrastingly, immunofluorescene analysis showed that the mean fluorescence intensity of FPN1 in RPMs was similar in both genotypes (Figure 2H and Supplementary Figure 2C). A plausible explanation for these findings is that the reduced RPM population in *Slc7a7*-deficient mice directly impacts the amount of FPN1, as the expression of this protein is restricted mainly to macrophages in the spleen (Hentze et al. 2010).

Overall, these data indicate that *Slc7a7*-deficient mice have a reduced population of RPMs, which is associated with increased apoptosis. Furthermore, *Slc7a7*-deficient RPMs exhibit increased expression of key RPM-associated genes involved in differentiation and hemoglobin scavenging.

Conditional deficiency of *Slc7a7* in macrophages does not affect iron homeostasis or the red pulp macrophage population in mice

To question the cell-autonomous effect of *Slc7a7* expression in macrophages on iron accumulation and macrophage development *in vivo*, we generated a myeloid cell-specific knockout mouse model in which Cre expression was specifically restricted to the myeloid lineage (*Slc7a7*^{LysM} KO mouse). Loss of *Slc7a7* gene expression was confirmed in BM-derived macrophages (BMDMs), alveolar macrophages and RPMs (Figure 3A). Myeloid-restricted deficiency of *Slc7a7* had no effect on RPM number (Figure 3B), and analysis of iron in the spleen and BM sections revealed similar levels in *Slc7a7*$^{LysM-/-}$ KO mice and control mice (Figure 3C). Finally, *Slc7a7*^{LysM} KO mice had no evident hyperferritinemia (Figure 3D). Taken together, these data suggest that macrophage *Slc7a7* is not the main player in iron redistribution and RPM homeostasis.

Erythrocytes from *Slc7a7*-deficient mice are more prone to erythrophagocytosis

The correlation between increased *CD163* and *SpiC* but not *Hmox1* expression in *Slc7a7*-deficient mice would suggest that while RPMs from *Slc7a7*-deficient mice might clear erythrocytes faster than in control animals, iron metabolism was not upregulated. To determine whether erythrophagocytosis was indeed elevated in *Slc7a7*-deficient macrophages, we performed an *ex vivo* assay to measure the erythrophagocytosis ratio in BMDMs from control and *Slc7a7*-deficient mice. Strikingly, when *Slc7a7*-deficient or control erythrocytes were co-incubated with BMDMs from the *Slc7a7*-deficient or control mice, *Slc7a7*-deficient erythrocytes were preferentially engulfed by both macrophage populations (Figure 4A). This observation supports the premise that the loss of *Slc7a7* in macrophages is not the main trigger of the increased erythrophagocytosis and macrophage iron accumulation in *Slc7a7*-deficient mice. If erythrocytes were the cause of the increased erythrophagocytosis and, in turn, iron redistribution, erythrocytes from *Slc7a7*-deficient mice would show signs of senescence. To test this, we investigated senescence signals and RBC fitness in *Slc7a7*-deficient mice. No significant changes were detected in the levels of annexin V or CD47 (a "self" label) on the erythrocyte membrane (Figure 4B,C) of *Slc7a7*-deficient mice, or on H_2O_2-induced ROS levels and RBC osmotic fragility (Figure 4D,E).

Slc7a7-deficient mice show stimulated erythropoiesis and lower levels of circulating erythropoietin

Our data show that erythrocytes from *Slc7a7*-deficient mice have a reduced cell size (MCV), which has been linked to stress erythropoiesis (Couch et al. 2018) and, in some cases, to elevated erythrophagocytosis (Bratosin et al. 1998; Gottlieb et al. 2012)(Chang Liao Blood, 2018). To address whether stress erythropoiesis might be the origin of the smaller MCV, we analyzed erythropoietic precursors in the BM of control and *Slc7a7*-deficient mice by flow cytometry. Of note, we found that the BM erythroblast number was severely reduced in *Slc7a7*-deficient mice. Specifically, proerythroblasts (region I), basophilic erythroblasts (region II), polychromatic erythroblasts (region III) and orthochromatic erythroblasts (region IV), were substabtially lower in number in *Slc7a7*-deficient mice than in control mice, whereas the percentage of mature RBCs (region V) was substantially higher (Figure 5A). These findings indicate that, despite having fewer erythrocyte precursors, *Slc7a7*-deficient mice and control mice have the same number of mature RBCs, suggesting hyperefficient erythropoiesis, which results in smaller erythrocytes. To test for a possible different expression pattern of CD44 and CD71 in control and *Slc7a7*-deficient mice, erythropoietic progenitors were also analyzed based on the expression of the transferrin receptor CD71. We found that the number of erythropoietic precursors at stages (I-IV) were substantially reduced in *Slc7a7*-deficient mice (Supplementary Figure 3). Because erythropoietin is the hormone responsible for promoting the survival, proliferation and differentiation of immature RBCs (Bhoopalan, Huang, and Weiss 2020), we measured the levels of circulating erythropoietin and total erythropoietin in kidney extracts from animals to question whether the smaller pro-erythroblast population in *Slc7a7*-deficient mice was associated with lower plasma erythropoietin. We found that plasma and total kidney erythropoietin levels were significantly lower in *Slc7a7*-deficient mice than in control mice (Figure 5B,C). Overall, these data suggest that the diminished systemic erythropoietin levels altered erythropoiesis.

Erythropoietin supplementation rescues the hematological defects in *Slc7a7*-deficient mice and reverses tissue iron accumulation

To study whether the reduced systemic erythropoietin was the main cause of the hematological abnormalities observed in *Slc7a7*-deficient mice, we administered erythropoietin (500 IU/kg) to both groups of mice over three consecutive days (Figure 6A) and measured erythropoietic precursors, blood parameters, erythrophagocytosis and iron content. In agreement with a previous study (Millot et al. 2010), administration of recombinant human erythropoietin significantly increased the spleen weight in both control and *Slc7a7*-deficient mice (Figure 6B) and partially recovered the RPM number (Figure 6C and Supplementary Figure 4A). Analysis of erythropoietic precursors showed that exogenous erythropoietin restored normal erythropoiesis in *Slc7a7*-deficient mice (Figure 6D and Supplementary Figure 4B), and analysis of blood parameters showed that MCV and other hemogram features were comparable between control and *Slc7a7*-deficient mice (Table 3). These findings further support the premise that reduced systemic erythropoietin underlies the hematological alterations of the mouse model of LPI. In this context, *Slc7a7*-deficient mice have a reduced glomerular filtration rate (Bodoy et al. 2019), suggesting that altered renal function could results in reduced erythropoietin production.

If the premise that a smaller RBC size triggers erythrophagocytosis in *Slc7a7*-deficient mice is correct, then erythrophagocytosis upon erythropoietin should not be compromised. Administration of recombinant erythropoietin restored normal erythrophagocytosis levels in *Slc7a7*-deficient mice (Figure 6E) and significantly reversed spleen iron accumulation (Figure 6F). Taken together, these results show that reduced erythropoietin is a major driver of the hematological abnormalities in a mouse model of LPI, which cause stress erythrophagocytosis and tissue iron accumulation.

Discussion

The immune and hematological complications resulting from multiple disorders, such as chronic kidney disease, in patients with LPI are the most life-threatening of this condition

(Ogier de Baulny et al. 2012). Although the disease can be managed by citrulline treatment and eventually ammonia scavengers, most patients ultimately die of end-stage renal disease and immune complications such as pulmonary alveolar proteinosis (Ogier de Baulny et al. 2012).

We show here that loss of *Slc7a7* in mice causes hyperferritinemia and reduced erythrocyte size, similar to what is seen in LPI (Habib et al. 2013; Ko et al. 2012). The tissue iron redistribution evident in *Slc7a7*-deficient mice has also been reported in some patients with LPI (Ceruti et al. 2007; Parto et al. 1994). The mechanisms underlying the development of hematological abnormalities in LPI, such as anemia and immune complications, have remained obscure. Here we used an inducible mouse model of LPI (Bodoy et al. 2019) in addition to a cell-specific (LysM-Cre) model to explore the hematological and immunological abnormalities of human LPI. We demonstrate that the expression of *Slc7a7* in macrophages is not a key player for macrophage homeostasis, as its ablation in the myeloid cell lineage fails to trigger a decrease in the RPM population. Moreover, *Slc7a7*^{LysM} KO mice did not show iron redistribution or hyperferritinemia. Although the expression of *Slc7a7* in RPMs was only reduced by ~50% in the LysM-Cre model, confirming the activity of LysM-Cre in RPM (Shi et al. 2018), it was, nevertheless, in the same range as for whole-body deletion of *Slc7a7*. Our findings in *Slc7a7*^{LysM} KO mice seems to exclude a cell-autonomous effect of *Slc7a7* in macrophages.

RPMs are responsible for senescent RBC scavenging, heme degradation and iron recycling (A-Gonzalez and Castrillo 2018). Upon defective recycling, iron is stored in macrophages, creating a toxic environment that can trigger cell death (Kovtunovych et al. 2010). We found that sorted RPMs from *Slc7a7*-deficient mice showed increased expression of genes involved in RPM differentiation and hemoglobin scavenging, which was reflected by increased erythrophagocytosis *ex vivo*. However, the increased erythrophagocytosis was evident only in *Slc7a7*-deficient mouse erythrocytes, and the macrophage genotype did not influence erythrophagocytosis. We speculate that enhanced erythrophagocytosis without increased heme catabolization (*Hmox-1*) may cause iron accumulation. Associations between

erythrophagocytosis and RPM death have been reported in *Hmox-1*-deficient mice and in the context of transfusion of aged RBCs, where RPMs undergo ferroptosis (iron-related cell death) due to increased ROS and lipid peroxidation (Kovtunovych et al. 2010; Youssef et al. 2018). However, further studies are required to elucidate the mechanisms underlying the increased hemoglobin capture but not its metabolization in RPMs of *Slc7a7*-deficient mice. Erythrocytes play an important role in erythrophagocytosis, as the presence of senescent signals in RBCs can trigger this process (Burger et al. 2012). We found that erythrocytes of *Slc7a7*-deficient mice do not display senescent signals such as increased annexin V or reduced CD47 staining. As far as we know, reduced MCV has not been fully linked to increased erythrophagocytosis; however, the abnormal shape of erythrocytes and hemolytic anemia have been reported to trigger RBC clearance (Bratosin et al. 2011; Chandrashekar and Soni 2012).

Exploring the mechanisms underlying reduced MCV, we found that erythropoiesis (RBC maturation) was dramatically altered in *Slc7a7*-deficient mice. Erythroblast precursors were significantly reduced in these mice, suggesting that erythroblast proliferation and maturation are altered after loss of *Slc7a7*. We also observed that plasma levels of erythropoietin, which promotes the survival, proliferation and differentiation of erythroid progenitors (Richmond, Chohan, and Barber 2005), was significantly lower in *Slc7a7*-deficient mice. Reduced circulating erythropoietin has been implicated in anemia and ineffective erythropoiesis, by downregulating Bcl-xL in erythroblasts, which is proposed to affect terminal erythroid differentiaion (Hafid-Medheb et al. 2003; Rhodes et al. 2005). Erythropoietin is produced specifically in Epo-producing renal cells located in the peritubular interstitium of the kidney (Pan et al. 2011). Erythropoietin synthesis is tightly linked to oxygen levels through the hypoxia-inducible factors, which are the main transcription factors that orchestrate erythropoietin production (Haase 2010). Importantly, in chronic kidney disease, a common complication of LPI, patients develop anemia as a result of deficient erythropoietin production (Batchelor et al. 2020). In this regard, we previously reported a reduced glomerular filtration rate in *Slc7a7*-deficient mice (Bodoy et al. 2019), suggesting a link between kidney function and the modest erythropoietin production in this model. However, histological analysis failed

to reveal the presence of kidney fibrosis or dysfunction. One explanation could be that the protocol used to develop LPI in mice is not sufficiently long to allow kidney failure to progress. Additional studies are needed to identify the mechanisms underlying the reduced levels of erythropoietin in kidney and plasma of *Slc7a7*-deficient mice.

We found that administration of erythropoietin was beneficial for the immune and hematological complications of LPI in *Slc7a7*-deficient mice. Exogenous administered erythropoietin rescued the reduced erythroid progenitor population and the reduced size of mature RBCs. To date, evidence that a reduced MCV can trigger erythrophagocytosis is limited. Erythropoietin supplementation demonstrated to rescue the reduced RBC size and erythrophagocytosis in *Slc7a7*-deficient mice, suggesting the possible effect of RBC size in triggering erythrophagocytosis. By contrast, three days of erythropoietin administration did not fully recover the RPM population in these animals. Erythropoietin supplementation in mice has been shown to increase macrophage populations within a period of three weeks (Hiram-Bab et al. 2015), suggesting that longer erythropoietin exposure will be beneficial for splenic RPM development in *Slc7a7*-deficient mice. Finally, we found that iron accumulation was also reversed upon erythropoietin administration, thus supporting our premise that increased erythrophagocytosis caused by reduced RBC size leads to substantial iron redistribution.

There have been previous attempts to treat the complications of end-stage renal disease and anemia in patients with LPI using erythropoietin supplementation. Nevertheless, the beneficial effect of erythropoietin in ameliorating the aformentioned symptoms was not observed (Tanner et al. 2007), likely because the disease was too far advanced when the erythropoietin administration began. In conclusion, we show that erythropoietin plays a unique role in the hematological complications in *Slc7a7*-deficient mice and that its deficiency has an indirect role on iron metabolism in this model of LPI. Normal erythropoietin levels are essential for proper iron distribution and metabolism in these animals. In this regard, a reduced RBC size would underlie increased RBC clearance, substantial iron accumulation, and loss of RPMs. The immune and hematologic complications of LPI have traditionally been considered independent entities (Ogier de Baulny et al. 2012). Our findings would support the notion that

management of the hematological complications in patients with LPI would prove beneficial for the reported hematologic and immunological abnormalities.

Author Contributions

J.G., F.S. and S.B. designed and performed experiments, and interpreted and analyzed data. J.G., S.B., and M.P. designed the research and wrote the manuscript, with input from all the authors. J.C. performed research. G.W., A.Z. and M.S. provided reagents and provided intellectual input.

The authors declare no competing financial interests.

Correspondence: Susanna Bodoy, Institute for Research in Biomedicine Barcelona, Baldiri Reixac, 12, Barcelona 08028, Spain; e-mail: susanna.bodoy@irbbarcelona.org; Manuel Palacín, Institute for Research in Biomedicine Barcelona, Baldiri Reixac, 12, Barcelona 08028, Spain; e-mail: manuel.palacin@irbbarcelona.org.

Acknowledgements

This work was supported by grants from the Spanish Ministry of Science and Innovation (grant SAF2015-64869-R-FEDER and RTI2018-094211-B-100), the Ramon Areces Foundation (I.O.F.R.ARECES), and the Generalitat de Catalunya (grant 2017 SGR 961). MS acknowledges grant RTI2018-101735-B-I00 from the Spanish Ministry of Science and Innovation. The EMBO Short-Term Fellowship Program facilitated the collaboration between international groups.

Figures, tables and legends

Table 1. Blood parameters from *Slc7a7* deficient and control mice.

Table 2. Kegg pathways showing differentially expressed pathways between red pulp macrophages from *Slc7a7* deficient and control mice.

Table 3. Blood parameters from *Slc7a7* deficient and control mice supplemented with exogenous erythropoietin.

Figure 1. *Slc7a7* deficiency results in tissue iron accumulation that is linked to macrophages. (A) Perl's Prussian Blue staining (to detect iron) of spleen and bone marrow (BM) sections from the indicated genotypes. Shown are representative images from 7 mice per group. Scale bars: 500 µm. Quantification of plasma ferritin (B) and plasma IL-6 (C). (D) Co-staining of F4/80 (shown in brown) of red pull macrophages and Perl's Prussian Blue (to detect iron) in spleen sections. Data are mean ± SEM. ** $P \leq 0.01$ between genotypes. *P*-values were calculated using two-tailed Student's *t*-test.

Figure 2. *Slc7a7* deficiency reduces the red pulp macrophage population in part through apoptosis and alters red pulp macrophage-associated gene expression. (A) Flow cytometry quantification of total number of monocytes (CD11b^{hi}, F4/80^{lo}), pre-red pulp macrophages (RPMs) (CD11b^{mild}, F4/80^{hi}) and RPMs (CD11b^{lo}, F4/80^{hi}) per spleen of the indicated genotypes. (B) Representative images of RPMs (F4/80 shown in dark) in spleen sections. Scale bar: 200 µm. (C) Quantification of circulating monocytes in peripheral blood. (D) Quantification of annexin V in RPMs (percentage of F4/80^{hi} and CD11b^{lo}). (E) Heatmap from sorted RPMs (F4/80^{hi}CD11b^{lo}) showing relative expression of key differentially-expressed RPM-associated genes (Haldar et al. 2014; Kohyama et al. 2009). Empty boxes indicate the *Slc7a7*$^{+/+}$ genotype and black boxes the *Slc7a7*$^{-/-}$ genotype. (F) Gene expression in sorted RPMs of indicated genes related to erythrophagocytosis and RPM differentiation. (G) FPN1 protein expression in total spleen extracts and relative fold-change (5-6 mice per group). (H) Mean fluorescence intensity (MFI) of FPN1 in RPMs (F4/80^{hi} and CD11b^{lo}). Data are mean ± SEM. * $P \leq 0.05$, ** $P \leq 0.01$, *** $P \leq 0.001$, **** $P \leq 0.0001$ between genotypes. *P*-values were calculated using two-tailed Students *t*-test.

Figure 3. *Slc7a7* deficiency in the myeloid lineage does not impact RPM development or tissue iron accumulation. (A) *Slc7a7* gene expression in bone marrow-derived macrophages (BMDMs), alveolar macrophages (AMs) and red pulp macrophages (RPMs) from *Slc7a7*$^{+/+}$, *Slc7a7*$^{-/-}$, *Slc7a7*$^{LysM+/+}$ and *Slc7a7*$^{LysM-/-}$ mice. (B) Flow cytometry quantification

of total number of RPMs per spleen (CD11b^{lo}, F4/80^{hi}). (C) Representative images (7 mice per group) of Perl's Prussian Blue staining (to detect iron) of spleens and bone marrow (BM) sections. Scale bars: 500 μm. (D) Quantification of plasma ferritin of the indicated genotype. Data are mean ± SEM. * $P \leq 0.05$, ** $P \leq 0.01$, *** $P \leq 0.001$, **** $P \leq 0.0001$ between genotypes. *P*-values were calculated using two-tailed Student's *t*-test.

Figure 4. Erythrocytes from *Slc7a7*-deficient mice are more prone to erythrophagocytosis. (A) Erythrophagocytosis assay. Bone marrow-derived macrophages were co-incubated with labeled erythrocytes. *Slc7a7*$^{+/+}$ erythrocytes (blue circles) were labeled with CellVue Claret, whereas *Slc7a7*$^{-/-}$ erythrocytes (orange circles) were labeled with PKH26. Left: Representative dot plots show the gating strategy for the Erythrophagocytosis assay. Right: Percentage of the cell populations analyzed. (B) Quantification of CD47-positive erythrocytes. (C) Quantification of annexin V-positive erythrocytes. (D) Left: Representative flow cytometry of reactive oxygen species (ROS) in red blood cells (RBCs). Right: Quantification of ROS levels in RBCs. (E) Osmotic fragility of RBCs. Data are mean ± SEM. *** $P \leq 0.001$, **** $P \leq 0.0001$ between genotypes. *P*-values were calculated using two-tailed Student's *t*-test.

Figure 5. *Slc7a7* deficiency results in defective erythropoiesis and reduced plasma erythropoietin. (A) Left: Representative dot plots show the gating strategy for erythroid progenitors (V, IV, III, II and I) (Chen et al. 2009) from the indicated genotype. Briefly, cells were first gated in TER119^{+} and further separated by CD44 *vs*. Forward Scatter (FSC-A). Right: Percentage of the cell populations analyzed. (B) Quantification of plasma erythropoietin. (C) Quantification of erythropoietin in kidney lysates. Data are represented as mean ± SEM. ** $P \leq 0.01$ between genotypes. *P*-values were calculated using two-tailed Students *t*-test.

Figure 6. Erythropoietin administration in *Slc7a7*-deficient mice restores normal erythropoiesis, erythrophagocytosis and tissue iron accumulation, but not red pulp macrophage numbers. (A) Graphical scheme of erythropoietin administration protocol in mice. (B) Spleen weights from the indicated genotypes administered with erythropoietin or vehicle. (C) Flow cytometry quantification of total number of red pulp macrophages per spleen (CD11b^{lo}, F4/80^{hi}) from the indicated mice administered with erythropoietin or vehicle. (D) Left: Representative dot plots show the gating strategy for erythroid progenitors (V, IV, III, II and I) (Chen et al. 2009) from the indicated genotype. Right: Percentage of the cell populations analyzed. (E) Erythrophagocytosis assay. Briefly, bone marrow-derived macrophages were co-incubated with labeled erythrocytes. *Slc7a7*$^{+/+}$ erythrocytes (blue circles) were labeled with CellVue Claret, whereas *Slc7a7*$^{-/-}$ erythrocytes (orange circles) were labeled with PKH26. Left: Representative dot plots show the gating strategy for the erythrophagocytosis assay. Right: Percentage of the cell populations analyzed. (F) Representative images (4 control and 6 *Slc7a7*$^{-/-}$ mice) of Perl's Prussian Blue staining (to detect iron) of spleen sections from the indicated genotype. Scale bars: 250 µm. Data are represented as mean ± SEM. * $P \leq 0.05$ and ** $P \leq 0.01$ between genotypes. *P*-values were calculated using two-tailed Students *t*-test.

Materials and methods

Animals

All animal work was conducted following established guidelines. The project (DARP n°9177) was favorably assessed by the Institutional Animal Care and Use Committee from Parc Científic de Barcelona (IACUC-PCB), and the IACUC considered that the project complies with standard ethical regulations and meets the requirements of current applicable legislation (RD 53/2013 Council Directive; 2010/63/UE; Order 214/1997/GC). *Slc7a7*$^{loxp/loxp}$ mice were generated by Eurogentec. To generate the *Slc7a7*$^{-/-}$ "*Slc7a7*-deficient" model, *Slc7a7*$^{loxp/loxp}$ animals (Bodoy et al. 2019) were crossed with UBC-Cre-ERT2 mice from The Jackson Laboratory. Male and female mice aged 12 weeks were used. Mice were housed in groups of 2–5 per cage and were kept under a 12 h dark-light period. Food and water were supplied *ad*

libitum. Animals were fed a standard diet (Teklad global 14% protein rodent maintenance diet) until tamoxifen induction, which consisted of a tamoxifen diet for one week. After the induction period, animals were maintained on a low-protein diet for 7–10 days prior to sacrifice. Control and *Slc7a7*-deficient littermates on a C57Bl6/J genetic background were sacrificed at 10–12 weeks of age by cervical dislocation. Tissues were dissected and flash-frozen in liquid nitrogen for RNA, protein, and iron quantification studies. For hematological and biochemical studies, blood was collected from a cardiac puncture in tubes containing either EDTA or heparin. The BM was flushed from femur and tibia bones.

Control and *Slc7a7*-deficient mice were intraperitoneally injected with recombinant human Epo (500 U/kg/day; R&D Systems) daily for three consecutive days. Mice in the control group were injected with an equivalent amount of saline.

Flow cytometry and cell sorting

For analysis of splenocytes and BM cells, crushed spleens and flushed BM samples were isolated and incubated with Fc-Block (anti-mouse CD16/32; ThermoFisher) for 30 min on ice. Cell suspensions were stained for the expression of CD71, CD11b, F4/80, TER119, and CD106 (all antibodies from BioLegend) for 30 min on ice. Flow cytometry was performed on a Gallios flow cytometer (BD Biosciences). For spleen analysis, crushed tissues were filtered through a 40-μm cell strainer and erythroid cells were removed by incubation with ammonium-chloride-potassium lysis buffer prior to the Fc-Block step. Cell sorting (purity >90%) was carried out using a FACS Aria II (BD Biosciences). For microarray analysis, spleens were prepared as described above and stained with anti-CD106, anti-CD11b and anti-F4/80 antibodies (ThermoFisher) for purified RPMs. For annexin V staining, RPMs and erythrocytes were incubated with 5 μL of Annexin V (Invitrogen) in 100 μL of Annexin V binding buffer (Invitrogen) for 15 min at room temperature (RT). Cells were then washed twice with PBS and re-suspended with Annexin V binding buffer. For RBC staining, cells were washed twice with PBS prior to the Fc-Block step. They were then stained with a CD47 antibody for 30 min on ice. Fluorescence was measured on Gallios flow cytometer.

Cell doublets were excluded from all analyses and, when possible, dead cells were excluded using DAPI staining. Data analysis was carried out using FlowJo™ Software.

In vitro erythrophagocytosis assay

To prepare primary BMDMs, cells obtained from mouse femurs and tibias were cultured for 7 days in the presence of 30% L-Cell conditioned medium (L929 SN) in Dulbecco's Modified Eagle's Medium (DMEM) supplemented with 10% fetal bovine serum (FBS), penicillin (50 U/mL) and streptomycin (50 µg/mL). BMDMs were plated 24 h before the experiment. On the day of the experiment, seeded BMDMs were activated with lipopolysaccharide (100 ng/mL) for 2 h and fresh RBCs were extracted from blood, washed, and labeled with CellVue® or PKH26 following the manufacturer's instructions. RBCs were then incubated with lipopolysaccharide-activated BMDMs for 2 min (10×10^6 RBC/1×10^6 BMDM) at 37ºC in a 5% CO_2 incubator. Macrophages were washed twice with PBS and finally incubated with an erythrolysis buffer (R&D Systems) to lyse non-ingested RBCs. Cells were then collected and analyzed by flow cytometry.

Histological sample preparation and analysis

Samples were fixed with neutral buffered formalin overnight at 4ºC. After fixation, bone tissue (femur) was washed with PBS and decalcified with Osteosoft® reagent at RT for a minimum of 15 days. All samples were embedded in paraffin. Paraffin-embedded tissue sections (2–3-µm thickness) were air-dried and further dried at 60ºC overnight. Bone sections were maintained at 60ºC for 48 h.

For iron staining, paraffin-embedded tissue sections were dewaxed and stained with Iron Stain Kit to identify iron pigment using the Dako Autostainer Plus. When combining iron staining with F4/80 immunohistochemistry, iron staining was performed first.

Prior to immunohistochemistry, sections were dewaxed, and epitopes were retrieved using proteinase K for 5 min at RT for rat monoclonal anti-F4/80 (eBioscience) staining. Quenching of endogenous peroxidase was performed with Peroxidase-Blocking Solution for

10 min at RT. Non-specific binding was blocked using 5% normal goat serum or normal donkey serum mixed with 2.5% bovine serum albumin diluted in the wash buffer, for 60 min at RT. The primary antibody dilution used was 1:2000, overnight. The secondary antibody used was a Biotin-SP (long spacer) AffiniPure Donkey Anti-Rat IgG (H+L) at 1:500 (in wash buffer) for 60 min, followed by amplification with Streptavidin-Peroxidase polymer at 1:1000. Antigen–antibody complexes were revealed with 3-3′-diaminobenzidine, with time exposure of 1 min. Sections were counterstained with hematoxylin and mounted with Toluene-Free Mounting Medium, using a Dako CoverStainer. Specificity of staining was confirmed with a rabbit IgG, polyclonal - Isotype control or Normal Rat IgG Control.

Brightfield images were acquired with a NanoZoomer-2.0 HT C9600 digital scanner (Hamamatsu) equipped with a 20× objective. All images were visualized with NDP.view 2 U123888-01 software using a gamma correction set at 1.8 in the image control panel of the software.

Tissue iron content

Liver and spleen non-heme iron content was measured using the bathophenanthroline colorimetric method (Torrance and Bothwell 1968). Mouse tissues were dried at 45ºC for 3 days, weighed, and then digested for 48 h at 65ºC in 10% TCA/10% HCl to allow deproteinization of non-heme iron. Diluted extracts were added to 0.01% bathophenanthroline disulfonic acid, 0.1% thioglycolic, 7M sodium acetate solution, and absorbance at 535 nm was measured using a Ultrospec 3100pro spectrophotometer (Amersham Biosciences). The iron content of samples was obtained by interpolation from a standard curve and calibration to the weight of dried material (Patel et al. 2002; Torrance and Bothwell 1968).

Plasma measurements

Commercial enzyme-linked immunosorbant assay kits were used to determine IL-6 (Abnova), erythropoietin (R&D Systems), ferritin (Abcam) proteins in fresh plasma.

Total kidney erythropoietin measurement

Kidneys were perfused with Hank's balanced salts solution, and total kidney extract were obtained by mechanical digestion with PBS supplemented with protein inhibitor (Protease Inhibitor Cocktail Set III, Merck).

Urine protein

Protein in urine was determined using the Pierce BCA Protein Assay Kit (Thermo Fisher Scientific).

Data and code availability

Microarray data have been deposited in the NCBI Gene Expression Omnibus repository under accession number GSE164827.

Microarray analysis

For gene expression analysis of RPMs, total RNA was isolated from purified cells using magnetic beads and the Agencourt RNA Clean XP Kit (Beckman Coulter). Quality and quantity were assessed using a Bioanalyzer 2100 (Agilent Technologies, Palo Alto, CA). Library preparation and amplification were performed as described (Gonzalez-Roca et al. 2010). RNA was amplified for 22 cycles and purified using the PureLink Quick PCR Purification Kit (Invitrogen) in the Genomic Facility of IRB Barcelona.

Pre-processing of microarray data

Microarray datasets were processed separately using the R (R Core 2019) packages affy (Gautier et al. 2004) and affyPLM (Bolstad et al. 2005) from Bioconductor (Gentleman et al. 2004). Raw cell files data were processed using RMA (Irizarry 2003) and annotated using the information available on the Affymetrix-Thermo Fisher web page. Standard quality controls were performed to identify abnormal samples regarding: a) spatial artefacts in the hybridization process (scan images and pseudo-images from probe-level models); b) intensity dependence of differences between chips (MvA plots); c) RNA quality (RNA digest plot); d) global intensity levels (boxplot of perfect match log-intensity distributions before and after normalization and

RLE plots); and e) anomalous intensity profile compared to the rest of the samples (NUSE plots, Principal Component Analysis).

Differential expression

Differential expression analysis was performed using a linear model with empirical shrinkage (Smyth 2004), as implemented in Limma R package (Ritchie et al. 2015). This model included the batch scanning for statistical control. Adjustment by multiple comparisons was performed using the Benjamini-Hochberg method (Benjamini and Hochberg 1995).

Biological enrichment analysis

Genes quantified in the microarray study were annotated according to the Broad Hallmark (Liberzon et al. 2015) gene set collection. Broad Hallmark sets were translated to mouse homologous genes using the R package biomaRt (Durinck et al. 2009).

Functional enrichment analyses were performed using a modification of ROAST (Wu et al. 2010), a rotation-based approach implemented in the Limma R package (Ritchie et al. 2015), which is especially suitable for small experiments. Such modifications were implemented to accommodate the proposed statistical re-standardization (Efron and Tibshirani 2007)in the ROAST algorithm, which enables its use for competitive testing (Goeman and Bühlmann 2007). The MaxMean (Efron and Tibshirani 2007) statistic was used for testing gene-set enrichment of Broad Hallmark. For each gene, the most variable probeset within each gene was used in these analyses (median absolute deviation). The results of these analyses were adjusted by multiple comparisons using the Benjamini-Hochberg False Discovery Rate method (Benjamini and Hochberg 1995).

Clustering and visualization

The expression of selected genes was graphically represented in a heatmap with the heatmap R package, using a blue to red gradation, where red indicates the highest expression and blue corresponds to the lowest expression values. Firstly, the expression data were summarized to the gene level using the most variable probeset mapping to the same gene (median absolute deviation), and expression values were centered and scaled gene-wise. Genes and samples were clustered using the Ward agglomeration method and the correlation and

Euclidean distances, respectively. To gain clarity in the graphic, the most extreme values were truncated to -1.5 and 1.5.

All analyses were carried out using R and Bioconductor.

RNA extraction and quantitative real-time PCR

Mice were killed by cervical dislocation, and tissues were immediately frozen for RNA isolation. Total RNA was isolated from purified cells using magnetic beads and the Agencourt RNA Clean XP Kit (Beckman Coulter). Quality and quantity were assessed using a Bioanalyzer 2100. RNA was amplified for 22 cycles and purified at the IRB Functional Genomic Facility using the PureLink Quick PCR Purification kit (Invitrogen). Amplification was performed using the ABI Prism 7900 HT real-time PCR platform (Applied Biosystems) and the SYBRc® Green PCR Master Mix. Gene expression levels were normalized with *18S* as housekeeping gene. The primer sequences are as follows: mouse *Spic* forward 5'-TCCGCAACCCAAGACTCTTCAA-3' and reverse 5'-GGGTTCTCTGTGGGTGACATTCCAT-3', mouse *Hmox1* forward 5'- ACATCGACAGCCCCACCAAGTTCAA -3' and reverse 5' – CTGACGAAGTGACGCCATCTGTGAG-3', mouse *Treml4* forward 5'-AAGCACAGCCACCATCTTTATG-3' and reverse 5'- GCACACAGAAAACTGACAGCA-3', mouse *Fpn1* forward 5'- AATGTGAACAAGAGCCCACCTG-3' and reverse 5-' GGACTGTCATATAGAGGAAAGCCAG-3', mouse *Vcam1* forward 5'-CCGGCATATACGAGTGTGAA-3' and reverse 5'-GATGCGCAGTAGAGTGCAAG-3'

, mouse *Cd163* forward 5'- GCTAGACGAAGTCATCTGCACTGG-3' and reverse 5'-TCAGCCTCAGAGACATGAACTCGG-3', mouse *Slc7a7* forward 5'-TCAACAGCACCAAGTATGAAGTG-3' and reverse 5'- AGCCCAGATGACCAGTGAGA-3' mouse *18S* forward 5'-GTAACCCGTTGAACCCCATT-3' and reverse 5'-CCATCCAATCGGTAGTAGCG-3'.

ROS measurement

ROS was measured as described (Zhang et al. 2018). Briefly, blood was extracted in heparin tubes and washed twice with PBS. Then 2×10^6 cells were resuspended in 100 µL PBS and incubated with 10 µL CM-H_2DCFDA (Invitrogen) with or without 10 µL H_20_2 for 15 min at 37ºC on a shaker. Fluorescence was measured in a FACSFusion II flow cytometer after washing twice with cold PBS.

Osmotic fragility assay

Osmotic fragility was assayed as described (Zhang et al. 2018). Briefly, 5 µL of blood was added to 200 µL of different concentrations of NaCl, incubated for 10 min at RT, and then centrifuged at 3000 × *g* for 5 min. Next, 150 µL of supernatant was placed in a 96-well plate and absorbance was measured at 540 nm. The fragility curve was constructed by plotting the percentage of hemolysis *versus* NaCl concentration.

Cultures of primary bone marrow macrophages (BMDMs)

BM cells from 12-week-old mice were flushed from femurs and tibiae. The cell suspension was lysed for 5 min in erythrolysis buffer (R&D Systems) at RT and then washed, resuspended, and cultured for 7 days in DMEM supplemented with 10% heat-inactivated FBS, 50 U/mL penicillin, 50 µg/mL streptomycin and 50 ng/mL of recombinant M-CSF (Peprotech) or 30% of L-Cell conditioned medium. Six days after seeding, cells were harvested and re-seeded with the previously mentioned conditioned medium for 24 h. To deplete arginine, arginine-free media was used (DMEM for SILAC, Thermo Fisher).

QUANTIFICATION AND STATISTICAL ANALYSIS

Data were analyzed using GraphPad Prism Version 8 software. Statistical analysis was performed using the Student's *t* test, as specified in each figure legend.

REFERENCES

A-Gonzalez, Noelia and Antonio Castrillo. 2018. "Origin and Specialization of Splenic Macrophages."

Cellular Immunology 330:151–58.
Batchelor, Elizabeth Katherine, Pinelopi Kapitsinou, Pablo E. Pergola, Csaba P. Kovesdy, and Diana I. Jalal. 2020. “Iron Deficiency in Chronic Kidney Disease: Updates on Pathophysiology, Diagnosis, and Treatment.” *Journal of the American Society of Nephrology* 31(3):456–68.
Benjamini, Yoav and Yosef Hochberg. 1995. “Controlling the False Discovery Rate: A Practical and Powerful Approach to Multiple Testing.” *Journal of the Royal Statistical Society: Series B (Methodological)* 57(1):289–300.
Bhoopalan, Senthil Velan, Lily Jun-Shen Huang, and Mitchell J. Weiss. 2020. “Erythropoietin Regulation of Red Blood Cell Production: From Bench to Bedside and Back.” *F1000Research* 9.
Bodoy, Sotillo, Espino-Guarch, Sperandeo, Ormazabal, Zorzano, Sebastio, Artuch, and Palacín. 2019. “Inducible Slc7a7 Knockout Mouse Model Recapitulates Lysinuric Protein Intolerance Disease.” *International Journal of Molecular Sciences* 20(21):5294.
Bolstad, BM, F. Collin, J. Brettschneider, K. Simpson, L. Cope, RA Irizarry, and TP Speet. 2005. “Quality Assessment of Affymetrix GeneChip Data.” Pp. 33–47 in *Bioinformatics and Computational Biology Solutions Using R and Bioconductor*, edited by R. Gentleman, V. Carey, W. Huber, R Irizarry, and S. Dudoit. New York, NY: Springer-Verlag.
Bratosin, D., J. Mazurier, J. P. Tissier, J. Estaquier, J. J. Huart, J. C. Ameisen, D. Aminoff, and J. Montreuil. 1998. “Cellular and Molecular Mechanisms of Senescent Erythrocyte Phagocytosis by Macrophages. A Review.” *Biochimie* 80(2):173–95.
Bratosin, Daniela, Jean-Pierre Tissier, Hélène Lapillonne, Olivier Hermine, Thierry Billette de Villemeur, Coralia Cotoraci, Jean Montreuil, and Cyril Mignot. 2011. “A Cytometric Study of the Red Blood Cells in Gaucher Disease Reveals Their Abnormal Shape That May Be Involved in Increased Erythrophagocytosis.” *Cytometry. Part B, Clinical Cytometry* 80(1):28–37.
Broxmeyer, Hal E. 2013. “Erythropoietin: Multiple Targets, Actions, and Modifying Influences for Biological and Clinical Consideration.” *Journal of Experimental Medicine* 210(2):205–8.
Burger, Patrick, Petra Hilarius-Stokman, Dirk De Korte, Timo K. Van Den Berg, and Robin Van Bruggen. 2012. “CD47 Functions as a Molecular Switch for Erythrocyte Phagocytosis.” *Blood* 119(23):5512–21.
Camaschella, Clara, Antonella Roetto, Angelita Calì, Marco De Gobbi, Giovanni Garozzo, Massimo Carella, Nunzia Majorano, Angela Totaro, and Paolo Gasparini. 2000. “The Gene TFR2 Is Mutated in a New Type of Haemochromatosis Mapping to 7q22.” *Nature Genetics* 25(1):14–15.
Ceruti, Michele, Giuseppe Rodi, Giulia M. Stella, Andrea Adami, Antonia Bolongaro, Aldo Baritussio, Ernesto Pozzi, and Maurizio Luisetti. 2007. “Successful Whole Lung Lavage in Pulmonary Alveolar Proteinosis Secondary to Lysinuric Protein Intolerance: A Case Report.” *Orphanet Journal of Rare Diseases* 2(1):1–7.
Chandrashekar, Vani and Mamta Soni. 2012. “Florid Erythrophagocytosis on the Peripheral Smear.” *Journal of Laboratory Physicians* 4(1):59–61.
Chen, Ke, Jing Liu, Susanne Heck, Joel A. Chasis, Xiuli An, and Narla Mohandas. 2009. “Resolving the Distinct Stages in Erythroid Differentiation Based on Dynamic Changes in Membrane Protein Expression during Erythropoiesis.” *Proceedings of the National Academy of Sciences* 106(41):17413–18.
Chow, Andrew, Matthew Huggins, Jalal Ahmed, Daigo Hashimoto, Daniel Lucas, Yuya Kunisaki, Sandra Pinho, Marylene Leboeuf, Clara Noizat, Nico Van Rooijen, Masato Tanaka, Zhizhuang Joe Zhao, Aviv Bergman, Miriam Merad, and Paul S. Frenette. 2013. “CD169 + Macrophages Provide a Niche Promoting Erythropoiesis under Homeostasis and Stress.” *Nature Medicine* 19(4):429–36.
Couch, Tyler A., Zachary C. Murphy, Jacquelyn Lillis, Michael Getman, Paul D. Kingsley, Ryo Kurita, Yukio Nakamura, and Laurie A. Steiner. 2018. “High-Level Setd8 Expression Is Important for Establishment of Normal Patterns of Erythroid Gene Expression and Is Essential for Stress Erythropoiesis.” *Blood* 132(Supplement 1):499–499.
Dhanakoti, S. N., J. T. Brosnan, G. R. Herzberg, and M. E. Brosnan. 1990. “Renal Arginine Synthesis: Studies in Vitro and in Vivo.” *American Journal of Physiology - Endocrinology and Metabolism* 259(3 22-3).
Dionisi-Vici, C., L. De Felice, M. El Hachem, S. Bottero, C. Rizzo, A. Paoloni, B. Goffredo, G. Sabetta, and M. Caniglia. 1998. “Intravenous Immune Globulin in Lysinuric Protein Intolerance.” *Journal of Inherited Metabolic Disease* 21(2):95–102.
Drakesmith, Hal, Elizabeta Nemeth, and Tomas Ganz. 2015. “Ironing out Ferroportin.” *Cell Metabolism* 22(5):777–87.
Durinck, Steffen, Paul T. Spellman, Ewan Birney, and Wolfgang Huber. 2009. “Mapping Identifiers for the Integration of Genomic Datasets with the R/ Bioconductor Package BiomaRt.” *Nature*

Protocols 4(8):1184–91.
Duval, Michel, Odile Fenneteau, Albert Faye, Dominique Emilie, Patricia Yotnda, Jean-claude Drapier, Nicole Schlegel, Ghislaine Sterkers, and Etienne Vilmer. 1999. “Intermittent Hemophagocytic Lymphohistiocytosis Is A.” *The Journal of Pediatrics* 134(2):8–11.
Efron, Bradley and Robert Tibshirani. 2007. “On Testing the Significance of Sets of Genes.” *The Annals of Applied Statistics* 1(1):107–29.
Fotiadis, Dimitrios, Yoshikatsu Kanai, and Manuel Palacín. 2013. “The SLC3 and SLC7 Families of Amino Acid Transporters.” *Molecular Aspects of Medicine* 34(2–3):139–58.
Gautier, Laurent, Leslie Cope, Benjamin M. Bolstad, and Rafael A. Irizarry. 2004. “Affy - Analysis of Affymetrix GeneChip Data at the Probe Level.” *Bioinformatics* 20(3):307–15.
Gentleman, Robert C., Vincent J. Carey, Douglas M. Bates, Ben Bolstad, Marcel Dettling, Sandrine Dudoit, Byron Ellis, Laurent Gautier, Yongchao Ge, Jeff Gentry, Kurt Hornik, Torsten Hothorn, Wolfgang Huber, Stefano Iacus, Rafael Irizarry, Friedrich Leisch, Cheng Li, Martin Maechler, Anthony J. Rossini, Gunther Sawitzki, Colin Smith, Gordon Smyth, Luke Tierney, Jean Y. H. Yang, and Jianhua Zhang. 2004. “Bioconductor: Open Software Development for Computational Biology and Bioinformatics.” *Genome Biology* 5(10):R80.
Goeman, Jelle J. and Peter Bühlmann. 2007. “Analyzing Gene Expression Data in Terms of Gene Sets: Methodological Issues.” *Bioinformatics* 23(8):980–87.
Gonzalez-Roca, Eva, Xabier Garcia-Albéniz, Silvia Rodriguez-Mulero, Roger R. Gomis, Karl Kornacker, and Herbert Auer. 2010. “Accurate Expression Profiling of Very Small Cell Populations” edited by S. Huang. *PLoS ONE* 5(12):e14418.
Gottlieb, Yehonatan, Orit Topaz, Lyora A. Cohen, Liat David Yakov, Tom Haber, Abigail Morgenstern, Avital Weiss, Karen Chait Berman, Eitan Fibach, and Esther G. Meyron-Holtz. 2012. “Physiologically Aged Red Blood Cells Undergo Erythrophagocytosis in Vivo but Not in Vitro.” *Haematologica* 97(7):994–1002.
Haase, Volker H. 2010. “Hypoxic Regulation of Erythropoiesis and Iron Metabolism.” *American Journal of Physiology-Renal Physiology* 299(1):F1–13.
Habib, Anasufiza, Zabedah Md Yunus, Nor Azimah Azize, Gaik Siew Ch’ng, Winnie Peitee Ong, Bee Chin Chen, Ho Torng Hsu, Ke Juin Wong, James Pitt, and Lock Hock Ngu. 2013. “Hyperexcretion of Homocitrulline in a Malaysian Patient with Lysinuric Protein Intolerance.” *European Journal of Pediatrics* 172(9):1277–81.
Hafid-Medheb, Khalid, Yvette Augery-Bourget, Marie-Nathalie Minatchy, Nicole Hanania, and Jacqueline Robert-Lézénès. 2003. “Bcl-XL Is Required for Heme Synthesis during the Chemical Induction of Erythroid Differentiation of Murine Erythroleukemia Cells Independently of Its Antiapoptotic Function.” *Blood* 101(7):2575–83.
Haldar, Malay, Masako Kohyama, Alex Yick-Lun So, Wumesh KC, Xiaodi Wu, Carlos G. Briseño, Ansuman T. Satpathy, Nicole M. Kretzer, Hisashi Arase, Namakkal S. Rajasekaran, Li Wang, Takeshi Egawa, Kazuhiko Igarashi, David Baltimore, Theresa L. Murphy, and Kenneth M. Murphy. 2014. “Heme-Mediated SPI-C Induction Promotes Monocyte Differentiation into Iron-Recycling Macrophages.” *Cell* 156(6):1223–34.
Hentze, Matthias W., Martina U. Muckenthaler, Bruno Galy, and Clara Camaschella. 2010. “Two to Tango: Regulation of Mammalian Iron Metabolism.” *Cell* 142(1):24–38.
Hiram-Bab, Sahar, Tamar Liron, Naamit Deshet-Unger, Moshe Mittelman, Max Gassmann, Martina Rauner, Kristin Franke, Ben Wielockx, Drorit Neumann, and Yankel Gabet. 2015. “Erythropoietin Directly Stimulates Osteoclast Precursors and Induces Bone Loss.” *The FASEB Journal* 29(5):1890–1900.
Irizarry, R. A. 2003. “Exploration, Normalization, and Summaries of High Density Oligonucleotide Array Probe Level Data.” *Biostatistics* 4(2):249–64.
Kawasumi, Hidenaga, Takahisa Gono, Yasushi Kawaguchi, Hirotaka Kaneko, Yasuhiro Katsumata, Masanori Hanaoka, Sayuri Kataoka, and Hisashi Yamanaka. 2014. “IL-6, IL-8, and IL-10 Are Associated with Hyperferritinemia in Rapidly Progressive Interstitial Lung Disease with Polymyositis/Dermatomyositis.” *BioMed Research International* 2014:1–6.
Klei, Thomas R. L., Sanne M. Meinderts, Timo K. van den Berg, and Robin van Bruggen. 2017. “From the Cradle to the Grave: The Role of Macrophages in Erythropoiesis and Erythrophagocytosis.” *Frontiers in Immunology* 8(FEB):73.
Ko, Jung Min, Choong Ho Shin, Sei Won Yang, Moon Woo Seong, Sung Sup Park, and Junghan Song. 2012. “The First Korean Case of Lysinuric Protein Intolerance: Presented with Short Stature and Increased Somnolence.” *Journal of Korean Medical Science* 27(8):961–64.
Kohyama, Masako, Wataru Ise, Brian T. Edelson, Peter R. Wilker, Kai Hildner, Carlo Mejia, William A. Frazier, Theresa L. Murphy, and Kenneth M. Murphy. 2009. “Role for Spi-C in the Development

of Red Pulp Macrophages and Splenic Iron Homeostasis." *Nature* 457(7227):318–21.
Korman, Stanley H., Annick Raas-Rothschild, Orly Elpeleg, and Alisa Gutman. 2002. "Hypocarnitinemia in Lysinuric Protein Intolerance." *Molecular Genetics and Metabolism* 76(1):81–83.
Kovtunovych, Gennadiy, Michael A. Eckhaus, Manik C. Ghosh, Hayden Ollivierre-Wilson, and Tracey A. Rouault. 2010. "Dysfunction of the Heme Recycling System in Heme Oxygenase 1-Deficient Mice: Effects on Macrophage Viability and Tissue Iron Distribution." *Blood* 116(26):6054–62.
Liberzon, Arthur, Chet Birger, Helga Thorvaldsdóttir, Mahmoud Ghandi, Jill P. Mesirov, and Pablo Tamayo. 2015. "The Molecular Signatures Database Hallmark Gene Set Collection." *Cell Systems* 1(6):417–25.
Millot, Sarah, Valérie Andrieu, Philippe Letteron, Saïd Lyoumi, Margarita Hurtado-Nedelec, Zoubida Karim, Olivier Thibaudeau, Samira Bennada, Jean-Luc Charrier, Sigismond Lasocki, and Carole Beaumont. 2010. "Erythropoietin Stimulates Spleen BMP4-Dependent Stress Erythropoiesis and Partially Corrects Anemia in a Mouse Model of Generalized Inflammation." *Blood* 116(26):6072–81.
Noguchi, Atsuko and Tsutomu Takahashi. 2019. "Overview of Symptoms and Treatment for Lysinuric Protein Intolerance." *Journal of Human Genetics* 64(9):849–58.
Ogier de Baulny, Hélène, Manuel Schiff, and Carlo Dionisi-Vici. 2012. "Lysinuric Protein Intolerance (LPI): A Multi Organ Disease by Far More Complex than a Classic Urea Cycle Disorder." *Molecular Genetics and Metabolism* 106(1):12–17.
Olonisakin, Tolani F., Tomeka Suber, Shekina Gonzalez-Ferrer, Zeyu Xiong, Hernán F. Peñaloza, Rick van der Geest, Yuting Xiong, David O. Osei-Hwedieh, Jesús Tejero, Matthew R. Rosengart, Wendy M. Mars, Daria Van Tyne, Andreas Perlegas, Samuel Brashears, Daniel B. Kim-Shapiro, Mark T. Gladwin, Michael A. Bachman, Eldad A. Hod, Claudette St. Croix, Yulia Y. Tyurina, Valerian E. Kagan, Rama K. Mallampalli, Anuradha Ray, Prabir Ray, and Janet S. Lee. 2021. "Stressed Erythrophagocytosis Induces Immunosuppression during Sepsis through Heme-Mediated STAT1 Dysregulation." *Journal of Clinical Investigation* 131(1).
Palacín, M, G. Borsani, and G. Sebastio. 2001. "The Molecular Bases of Cystinuria and Lysinuric Protein Intolerance." *Current Opinion in Genetics & Development* 11(3):328–35.
Palacín, Manuel, Giuseppe Borsani, Gianfranco Sebastio, Manuel Palacín, Giuseppe Borsani, Gianfranco Sebastio, Manuel Palacín, Giuseppe Borsani, Gianfranco Sebastio, Manuel Palacín, Giuseppe Borsani, and Gianfranco Sebastio. 2001. "The Molecular Bases of Cystinuria and Lysinuric Protein Intolerance." *Current Opinion in Genetics and Development* 11(3):328–35.
Palacín, Manuel, Virginia Nunes, Mariona Font-Llitjós, Maite Jiménez-Vidal, Joana Fort, Emma Gasol, Marta Pineda, Lidia Feliubadaló, Josep Chillarón, and Antonio Zorzano. 2005. "The Genetics of Heteromeric Amino Acid Transporters." *Physiology* 20(2):112–24.
Pan, Xiaoqing, Norio Suzuki, Ikuo Hirano, Shun Yamazaki, Naoko Minegishi, and Masayuki Yamamoto. 2011. "Isolation and Characterization of Renal Erythropoietin-Producing Cells from Genetically Produced Anemia Mice." *PloS One* 6(10).
Parenti, Giancarlo, Gianfranco Sebastio, Pietro Strisciuglio, Barbara Incerti, Carmine Pecoraro, Luigi Terracciano, and Generoso Andria. 1995. "Lysinuric Protein Intolerance Characterized by Bone Marrow Abnormalities and Severe Clinical Course." *The Journal of Pediatrics* 126(2):246–51.
Parto, K., J. Maki, L. J. Pelliniemi, and O. Simell. 1994. "Abnormal Pulmonary Macrophages in Lysinuric Protein Intolerance: Ultrastructural, Morphometric, and x-Ray Microanalytic Study." *Archives of Pathology and Laboratory Medicine* 118(5):536–41.
Patel, Bharatkumar N., Robert J. Dunn, Suh Young Jeong, Qinzhang Zhu, Jean Pierre Julien, and Samuel David. 2002. "Ceruloplasmin Regulates Iron Levels in the CNS and Prevents Free Radical Injury." *Journal of Neuroscience* 22(15):6578–86.
Paulson, Robert F., Baiye Ruan, Siyang Hao, and Yuanting Chen. 2020. "Stress Erythropoiesis Is a Key Inflammatory Response." *Cells* 9(3):634.
Perkins, Christopher P., Vernon Mar, John R. Shutter, Juan Del Castillo, Dimitry M. Danilenko, Eugene S. Medlock, Ian L. Ponting, Melissa Graham, Kevin L. Stark, Yi Zuo, James M. Cunningham, and Robert A. Bosselman. 1997. "Anemia and Perinatal Death Result from Loss of the Murine Ecotropic Retrovirus Receptor MCAT-1." *Genes and Development* 11(7):914–25.
Priwitzerova, Monika, Guangjun Nie, Alex D. Sheftel, Dagmar Pospisilova, Vladimir Divoky, and Prem Ponka. 2005. "Functional Consequences of the Human DMT1 (SLC11A2) Mutation on Protein Expression and Iron Uptake." *Blood* 106(12):3985–87.
R Core, Team. 2019. "R: A Language and Environment for Statistical Computing. R Foundation for Statistical Computing." *Vienna, Austria*. Retrieved (https://www.r-project.org/.).
Rhodes, Melissa M., Prapaporn Kopsombut, Maurice C. Bondurant, James O. Price, and Mark J.

Koury. 2005. “Bcl-XL Prevents Apoptosis of Late-Stage Erythroblasts but Does Not Mediate the Antiapoptotic Effect of Erythropoietin.” *Blood* 106(5):1857–63.
Richmond, Terri D., Manprit Chohan, and Dwayne L. Barber. 2005. “Turning Cells Red: Signal Transduction Mediated by Erythropoietin.” *Trends in Cell Biology* 15(3):146–55.
Ritchie, Matthew E., Belinda Phipson, Di Wu, Yifang Hu, Charity W. Law, Wei Shi, and Gordon K. Smyth. 2015. “Limma Powers Differential Expression Analyses for RNA-Sequencing and Microarray Studies.” *Nucleic Acids Research* 43(7):e47.
Rosário, Cristina, Gisele Zandman-Goddard, Esther G. Meyron-Holtz, David P. D’Cruz, and Yehuda Shoenfeld. 2013. “The Hyperferritinemic Syndrome: Macrophage Activation Syndrome, Still’s Disease, Septic Shock and Catastrophic Antiphospholipid Syndrome.” *BMC Medicine* 11(1):185.
Rotoli, Bianca Maria, Amelia Barilli, Rossana Visigalli, Francesca Ferrari, and Valeria Dall’Asta. 2020. “Y+LAT1 and Y+LAT2 Contribution to Arginine Uptake in Different Human Cell Models: Implications in the Pathophysiology of Lysinuric Protein Intolerance.” *Journal of Cellular and Molecular Medicine* 24(1):921–29.
Rotoli, Bianca Maria, Amelia Barilli, Rossana Visigalli, Filippo Ingoglia, Marco Milioli, Maria Di Lascia, Benedetta Riccardi, Paola Puccini, Valeria Dall’Asta, Maria Di Lascia, Benedetta Riccardi, Paola Puccini, and Valeria Dall’Asta. 2018. “Downregulation of SLC7A7 Triggers an Inflammatory Phenotype in Human Macrophages and Airway Epithelial Cells.” *Frontiers in Immunology* 9(MAR):508.
Shi, Jiayuan, Li Hua, Danielle Harmer, Peishan Li, and Guangwen Ren. 2018. “Cre Driver Mice Targeting Macrophages.” Pp. 263–75 in *Methods in molecular biology (Clifton, N.J.)*. Vol. 1784. NIH Public Access.
Simell, Olli. 2001. “Lysinuric Protein Intolerance and Other Cationic Aminoacidurias.” P. Chapter 192 in *The Metabolic and Molecular Bases of Inherited Disease*, edited by C. R. Scriver, B. Childs, A. Beaudet, D. Valle, K. Kinzler, and B. Vogelstein.
Smyth, Gordon K. 2004. “Linear Models and Empirical Bayes Methods for Assessing Differential Expression in Microarray Experiments.” *Statistical Applications in Genetics and Molecular Biology* 3(1).
Tanner, Laura M., Kirsti Näntö-Salonen, Harri Niinikoski, Timo Jahnukainen, Päivi Keskinen, Heikki Saha, Kristiina Kananen, Antero Helanterä, Martti Metso, Marjatta Linnanvuo, Kirsi Huoponen, and Olli Simell. 2007. “Nephropathy Advancing to End-Stage Renal Disease: A Novel Complication of Lysinuric Protein Intolerance.” *Journal of Pediatrics* 150(6).
Theurl, Igor, Ingo Hilgendorf, Manfred Nairz, Piotr Tymoszuk, David Haschka, Malte Asshoff, Shun He, Louisa M. S. Gerhardt, Tobias A. W. Holderried, Markus Seifert, Sieghart Sopper, Ashley M. Fenn, Atsushi Anzai, Sara Rattik, Cameron McAlpine, Milan Theurl, Peter Wieghofer, Yoshiko Iwamoto, Georg F. Weber, Nina K. Harder, Benjamin G. Chousterman, Tara L. Arvedson, Mary McKee, Fudi Wang, Oliver M. D. Lutz, Emanuele Rezoagli, Jodie L. Babitt, Lorenzo Berra, Marco Prinz, Matthias Nahrendorf, Guenter Weiss, Ralph Weissleder, Herbert Y. Lin, and Filip K. Swirski. 2016. “On-Demand Erythrocyte Disposal and Iron Recycling Requires Transient Macrophages in the Liver.” *Nature Medicine* 22(8):945–51.
Torrance, J. D. and T. H. Bothwell. 1968. “A Simple Technique for Measuring Storage Iron Concentrations in Formalinised Liver Samples.” *The South African Journal of Medical Sciences* 33(1):9–11.
Torrents, David, Juha Mykkänen, Marta Pineda, Lidia Feliubadaló, Raúl Estévez, Rafael de Cid, Pablo Sanjurjo, Antonio Zorzano, Virginia Nunes, Kirsi Huoponen, Arja Reinikainen, Olli Simell, Marja-Liisa Savontaus, Pertti Aula, and Manuel Palacín. 1999. “Identification of SLC7A7, Encoding Y+LAT-1, as the Lysinuric Protein Intolerance Gene.” *Nature Genetics* 21(3):293–96.
Wu, Di, Elgene Lim, François Vaillant, Marie Liesse Asselin-Labat, Jane E. Visvader, and Gordon K. Smyth. 2010. “ROAST: Rotation Gene Set Tests for Complex Microarray Experiments.” *Bioinformatics* 26(17):2176–82.
Youssef, Lyla A., Abdelhadi Rebbaa, Sergey Pampou, Stuart P. Weisberg, Brent R. Stockwell, Eldad A. Hod, and Steven L. Spitalnik. 2018. “Increased Erythrophagocytosis Induces Ferroptosis in Red Pulp Macrophages in a Mouse Model of Transfusion.” *Blood* 131(23):2581.
Zhang, De-liang, Jian Wu, Binal N. Shah, Katja C. Greutélaers, Manik C. Ghosh, Hayden Ollivierre, Xin-zhuan Su, Philip E. Thuma, George Bedu-Addo, Frank P. Mockenhaupt, Victor R. Gordeuk, and Tracey A. Rouault. 2018. “Erythrocytic Ferroportin Reduces Intracellular Iron Accumulation, Hemolysis, and Malaria Risk.” *Science* 359(6383):1520–23.
Zhu, B. M., S. K. McLaughlin, Risu Na, Jie Liu, Yongzhi Cui, Cyril Martin, Akiko Kimura, Gertraud W. Robinson, Nancy C. Andrews, and Lothar Hennighausen. 2008. “Hematopoietic-Specific Stat5-Null Mice Display Microcytic Hypochromic Anemia Associated with Reduced Transferrin

Receptor Gene Expression.” *Blood* 112(5):2071–80.

Figure 1

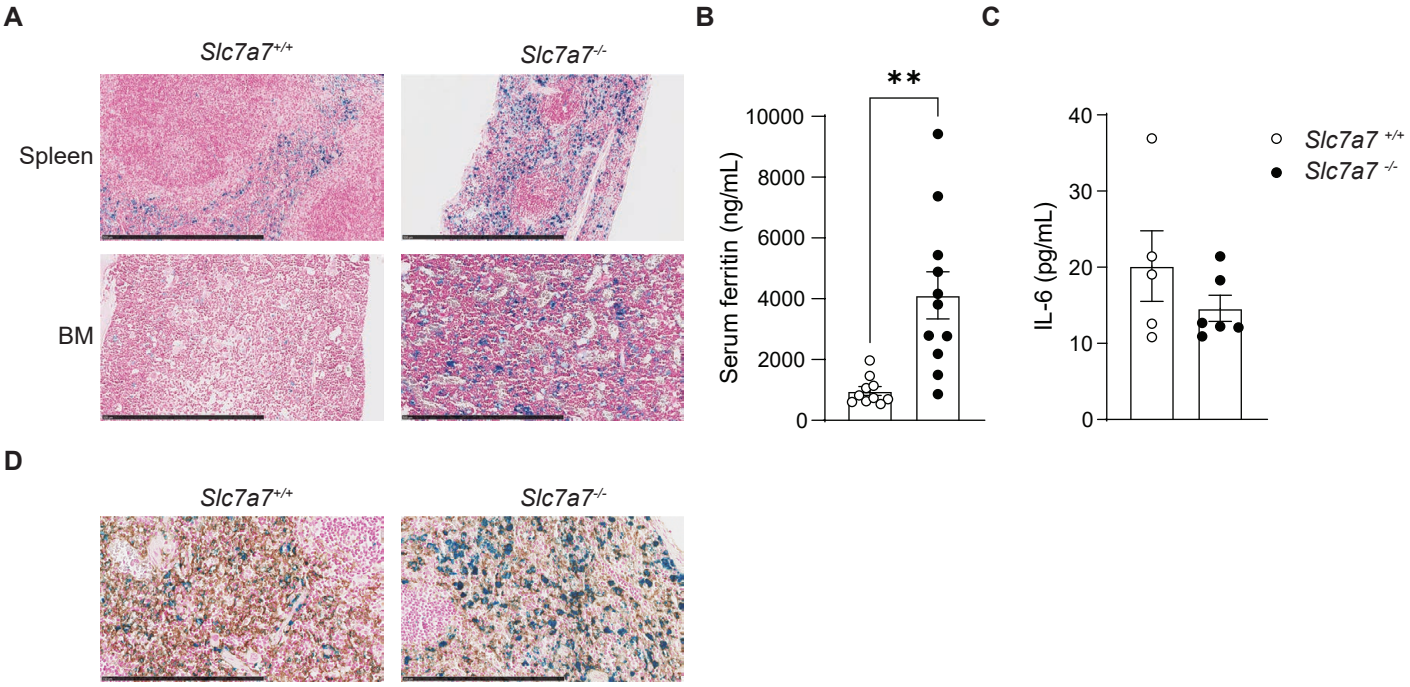
A
Slc7a7+/+
Slc7a7-/-
Spleen
BM
B
**
Serum ferritin (ng/mL)
10000
8000
6000
4000
2000
0
C
IL-6 (pg/mL)
40
30
20
10
0
Slc7a7 +/+
Slc7a7 -/-
D
Slc7a7+/+
Slc7a7-/-

Figure 2

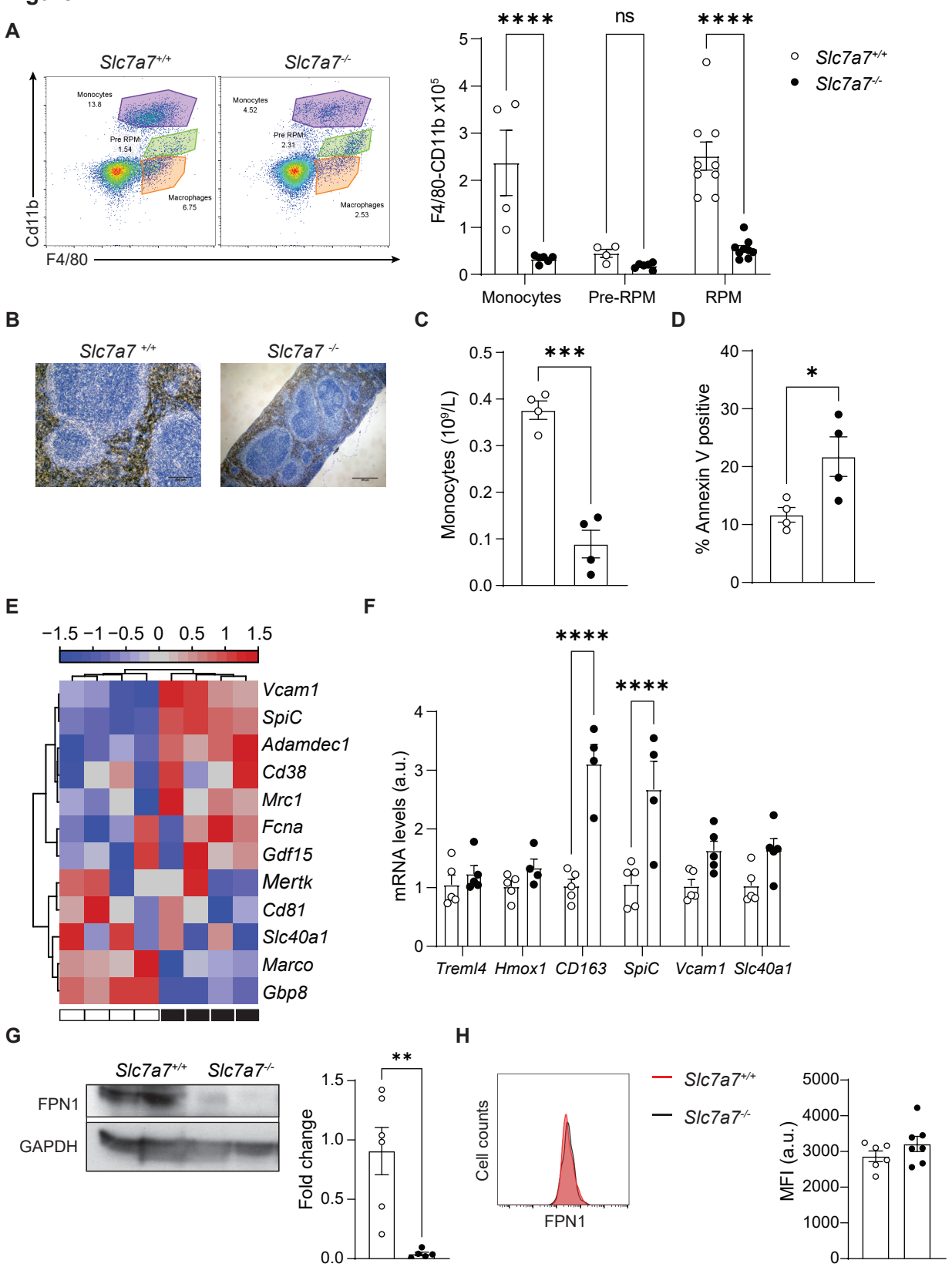
A
Slc7a7+/+
Slc7a7-/-
Monocytes 13.8
Pre RPM 1.54
Macrophages 6.75
Monocytes 4.52
Pre RPM 2.31
Macrophages 2.53
Cd11b
F4/80
F4/80-CD11b x10^5
****
ns
****
Monocytes
Pre-RPM
RPM
B
Slc7a7 +/+
Slc7a7 -/-
C
Monocytes (10^9/L)
***
D
% Annexin V positive
*
E
−1.5 −1 −0.5 0 0.5 1 1.5
Vcam1
SpiC
Adamdec1
Cd38
Mrc1
Fcna
Gdf15
Mertk
Cd81
Slc40a1
Marco
Gbp8
F
mRNA levels (a.u.)
****
****
Treml4
Hmox1
CD163
SpiC
Vcam1
Slc40a1
G
Slc7a7+/+
Slc7a7-/-
FPN1
GAPDH
Fold change
**
H
Cell counts
FPN1
Slc7a7+/+
Slc7a7-/-
MFI (a.u.)

Figure 3

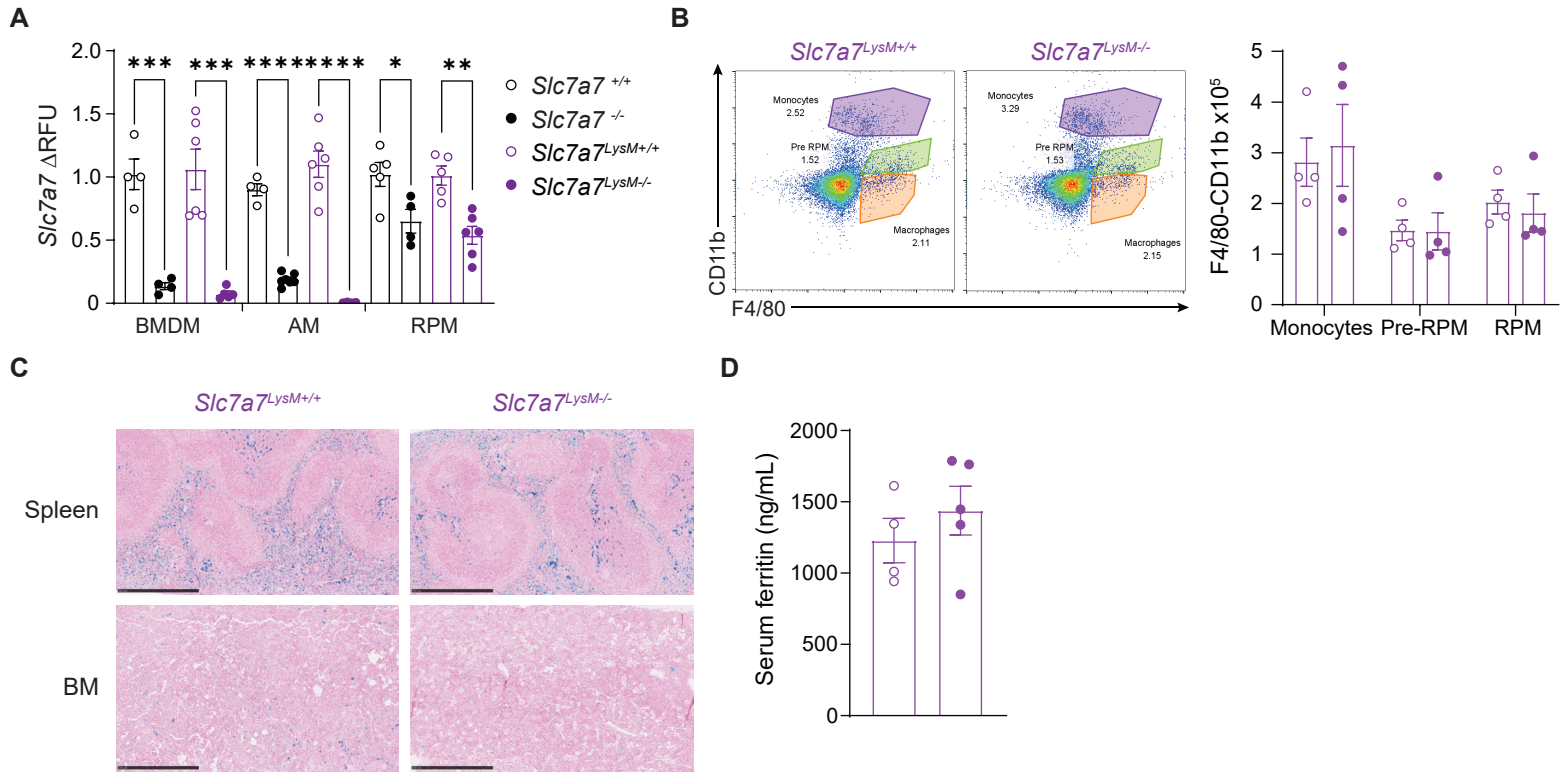
A
Slc7a7 ΔRFU
2.0
1.5
1.0
0.5
0
***
***
****
*
**
BMDM
AM
RPM
Slc7a7 +/+
Slc7a7 -/-
Slc7a7LysM+/+
Slc7a7LysM-/-
B
Slc7a7LysM+/+
Slc7a7LysM-/-
Monocytes 2.52
Pre RPM 1.52
Macrophages 2.11
Monocytes 3.29
Pre RPM 1.53
Macrophages 2.15
CD11b
F4/80
F4/80-CD11b x10^5
5
4
3
2
1
0
Monocytes
Pre-RPM
RPM
C
Slc7a7LysM+/+
Slc7a7LysM-/-
Spleen
BM
D
Serum ferritin (ng/mL)
2000
1500
1000
500
0

Figure 4

A

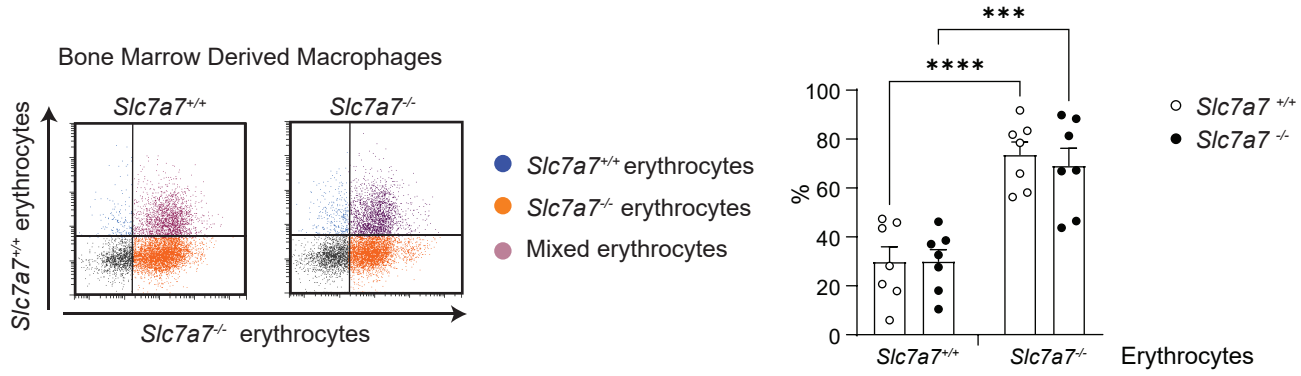

B

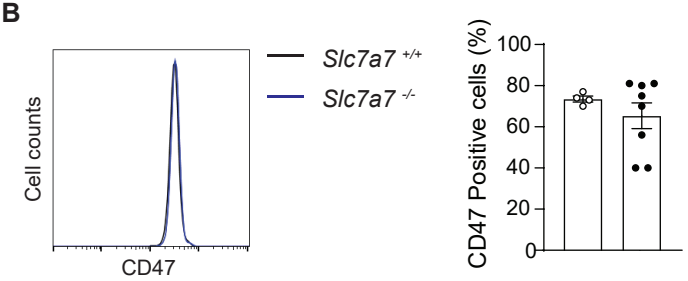

C

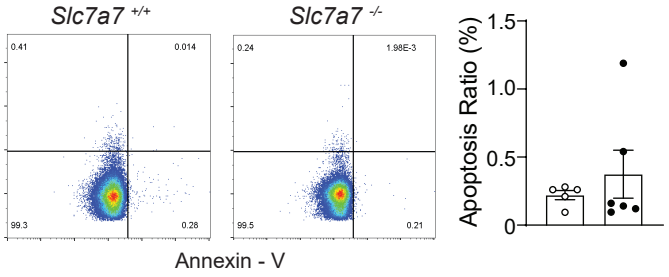

D

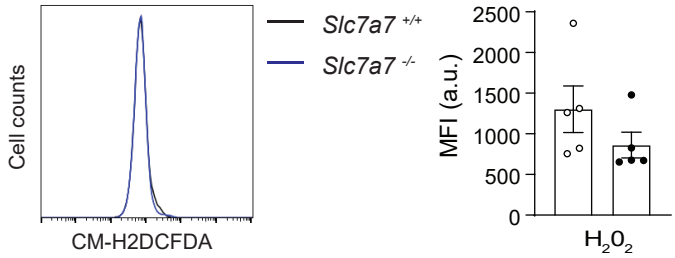

E

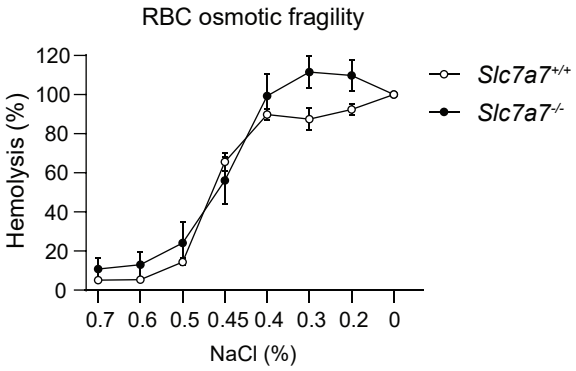

Figure 5

A

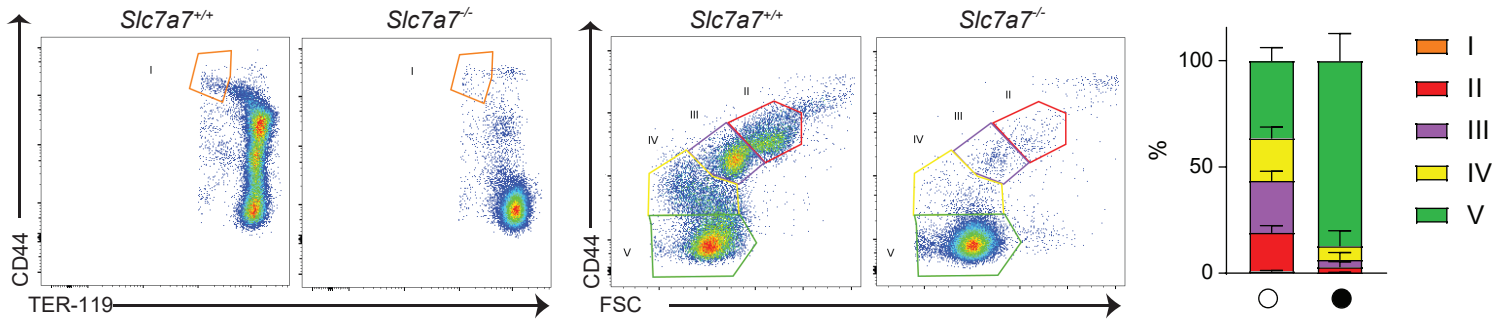
Slc7a7+/+
Slc7a7-/-
CD44
TER-119
FSC
I
II
III
IV
V
%
100
50
0

B

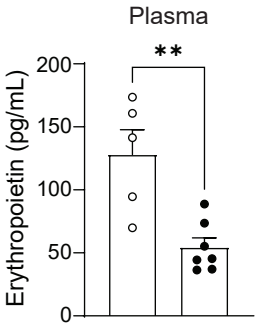
Plasma
**
Erythropoietin (pg/mL)
200
150
100
50
0

C

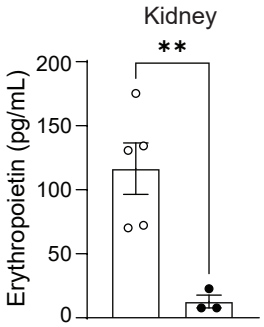
Kidney
**
Erythropoietin (pg/mL)
200
150
100
50
0

Figure 6

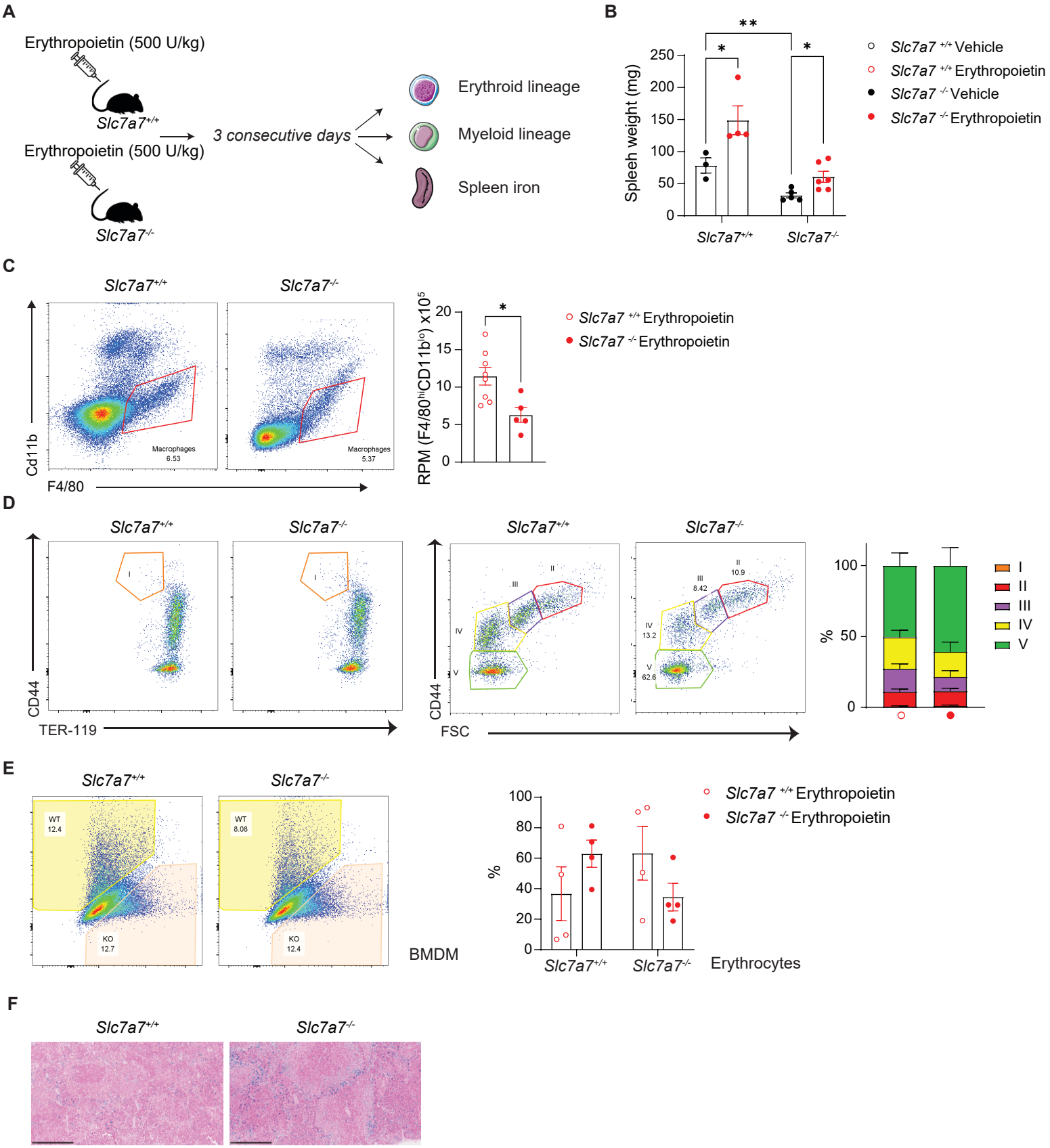
A
Erythropoietin (500 U/kg)
Slc7a7+/+
3 consecutive days
Erythropoietin (500 U/kg)
Slc7a7-/-
Erythroid lineage
Myeloid lineage
Spleen iron
B
Spleen weight (mg)
Slc7a7+/+
Slc7a7-/-
Slc7a7 +/+ Vehicle
Slc7a7 +/+ Erythropoietin
Slc7a7 -/- Vehicle
Slc7a7 -/- Erythropoietin
C
Slc7a7+/+
Slc7a7-/-
Cd11b
F4/80
Macrophages 6.53
Macrophages 5.37
RPM (F4/80hiCD11blo) x10^5
Slc7a7 +/+ Erythropoietin
Slc7a7 -/- Erythropoietin
D
CD44
TER-119
FSC
%
I
II
III
IV
V
E
WT 12.4
KO 12.7
WT 8.08
KO 12.4
BMDM
Erythrocytes
F

Table 1

Genotype	Hb, g/dL	HCT, %	MCH, pg	MCV, fL	RBC, 10^6/µL
Slc7a7$^{+/+}$	11.08 ± 0.96	32.09 ± 3.1	14.59 ± 0.31	42.37 ± 1.01	7.19 ± 0.82
Slc7a7$^{-/-}$	10.09 ± 1.34	29.09 ± 2.91	13.55 ± 0.69 **	39.16 ± 0.95 ***	7.42 ± 0.63

Table 2

Hallmark Term	PValue	NES
UV response DN	0.001	2.584
Xenobiotic metabolism	0.044	2.025
Complement	0.026	1.883
Wnt-β catenin signaling	0.012	1.855
Protein secretion	0.043	1.624
G2M checkpoint	0	-3.917
IL2 STAT5 signaling	0	-3.311
Mitotic spindle	0	-3.07
Inflammatory response	0	-3.049
IL6 JAK STAT3 signaling	0	-2.797
TNF-α signaling via NFKB	0.001	-2.599
Interferon γ response	0.001	-2.584
Allograft rejection	0	-2.569
Estrogen response late	0.007	-2.518
KRAS signaling up	0.007	-2.509
E2F Targets	0	-2.469
Angiogenesis	0.005	-2.263
Apoptosis	0	-2.132
Apical Junction	0.009	-2.13
Unfolded protein response	0.009	-2.099
Estrogen response early	0.017	-1.981
Glycolysis	0.054	-1.975
mTORC1 SIGNALING	0.033	-1.913
P53 Pathway	0.094	-1.637
Fatty acid metabolism	0.131	-1.557
Heme metabolism	0.187	-1.412

Table 3

Genotype	Hb, g/dL	HCT, %	MCH, pg	MCV, fL	RBC, 10^6/µL
Slc7a7$^{+/+}$	13.62 ± 2.36	41.35 ± 6.59	15.12 ± 0.42	46.02 ± 1.07	8.99 ± 1.43
Slc7a7$^{-/-}$	15 ± 0.71	45.86 ± 1.3	14.66 ± 0.09	44.76 ± 0.73	10.26 ± 0.44